Advanced imaging and spectroscopy techniques for body magnetic resonance

Heer, P. de

5

MR OF MULTI-ORGAN INVOLVEMENT IN THE METABOLIC SYNDROME

5 MR OF MULTI-ORGAN INVOLVEMENT IN THE METABOLIC SYNDROME

Adapted from Magnetic Resonance Imaging Clinics of North America. 2015 Feb;23(1):41-58.

Authors

Maurice B. Bizino, MD,[1] Michael L. Sala, MD,[1] Paul de Heer, MSc,[2] Pieternel van der Tol, MSc,[1] Jan W.A. Smit, MD, PhD,[3] Andrew G. Webb, PhD,[2] Albert de Roos, MD, PhD,[2] Hildo J. Lamb, MD, PhD[1]

[1] Department of Radiology, Leiden University Medical Center, Albinusdreef 2, Leiden 2333 ZA, The Netherlands
[2] C.J. Gorter Center for High Field MRI, Department of Radiology, Leiden University Medical Center, Albinusdreef 2, Leiden 2333 ZA, The Netherlands
[3] Division of Endocrinology, Department of Medicine, Radboud University Medical Centre, PO Box 9101, 6500 HB, Nijmegen, The Netherlands

KEY POINTS

- State-of-the-art magnetic resonance (MR) technologies provide whole-body assessment of metabolic syndrome (MetS) pathophysiology and complications.
- MRI and MR spectroscopy image and quantify ectopic lipid accumulation, such as pericardial/perivascular fat, visceral abdominal fat, and fatty infiltration of organs, associated with adverse outcome.
- By using MR elastography, T1-mapping, phosphorus MR spectroscopy, and diffusion-weighted imaging, MR can assist in staging nonalcoholic fatty liver disease.
- Using cardiac MRI, spectroscopy, and mapping techniques, key features of diabetic cardiomyopathy, such as diastolic dysfunction, left ventricular hypertrophy, myocardial steatosis and fibrosis, can be quantified.
- Novel MR techniques, such as magnetization transfer imaging and diffusion tensor imaging, demonstrate microstructural brain damage in MetS.

INTRODUCTION

Epidemiology

About one-third of the United States population of 20 years or older has metabolic syndrome (MetS) and its prevalence increases with advancing age and body mass index,[1] stressing its tight association with the obesity epidemic.

Definition

Diagnosis of MetS requires positive identification of at least 3 out of 5 criteria displayed in Table 1.

Table 1 Diagnosis of MetS

MetS Criteria (NCEP-ATP III Criteria)	Definition
Abdominal obesity: waist circumference	Men > 40 inches Women > 35 inches
Increased plasma triglyceride level	> 150 mg/dL
Decreased plasma HDL level	Men < 40 mg/dL Women < 50 mg/dL
Elevated blood pressure	> 130/85 mm Hg
Increased plasma fasting glucose	> 100 mg/dL

As such, approximately 90% of type 2 diabetes mellitus (DM2) patients have MetS.[1] Patients with MetS are heterogeneous in nature with varying risk of disease and consequently require personalized care, for example, by MR prognosis, in terms of future cardiovascular and cerebrovascular events (Figure 1).[2]

MRI of Multi-Organ Involvement in the Metabolic Syndrome

MetS is a systemic disease with complex pathophysiology including insulin resistance, atherogenic dyslipidemia, hypertension, ectopic lipid accumulation, low-grade inflammation, prothrombotic state, and fibrosis resulting in end-organ damage.[3] MRI and magnetic resonance spectroscopy (MRS) can be used to quantify ectopic lipid accumulation. Importantly, as shown in Figure 2, functional and structural consequences of MetS can be evaluated with MR on a whole body level. In the liver, several techniques — ranging from MRS and water-fat imaging to magnetic resonance elastography (MRE) and T1 mapping —are used to quantify hepatic steatosis and differentiate between stages of nonalcoholic fatty liver disease (NAFLD). In parallel, cardiac MR can quantify myocardial steatosis and associated complications, such as diastolic dysfunction and fibrosis. In the brain, magnetization transfer imaging and diffusion tensor imaging (DTI) can detect microstructural brain damage associated with MetS. The involvement of various other organs ranging from the kidney to pancreas and skeletal muscle can be assessed with MR.

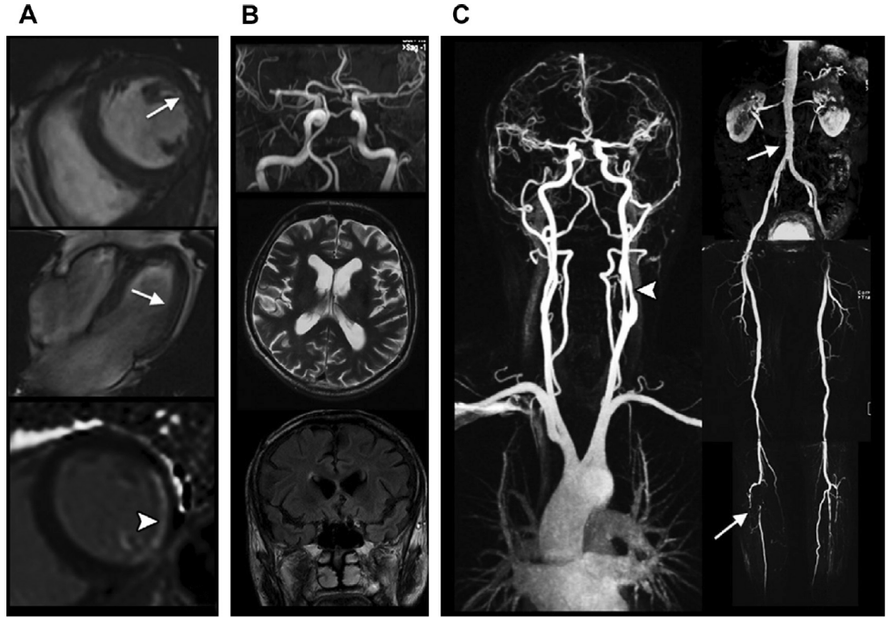

FIGURE 1. Clinical whole-body MR for risk estimation of future cardiovascular events. Images acquired in a 74-year old man with a 21-year history of type 2 diabetes mellitus. (A) Cardiac MRI involving cine imaging (top and middle) showing hypokinesia in the anterolateral segment (arrow). The bottom image is a late gadolinium enhanced image displaying subendocardial enhancement (arrowhead) consistent with myocardial infarction. **(B)** Cerebral arteries using time-of-flight angiography (top), an axial T2-weighted brain image (middle) and a coronal fluid-attenuated inversion-recovery image (bottom). These images show no overt brain abnormalities associated with the metabolic syndrome (MetS). **(C)** Contrast-enhanced MR angiograms of carotid arteries (left) and abdominal and lower extremity arteries (right) with arrowhead and arrows indicating stenosis owing to atherosclerotic disease. Using this 60-minute MR protocol, future cardiac and cerebrovascular events can be predicted in DM patients with higher accuracy compared with clinical characteristics.[1] (From Bamberg F, Parhofer KG, Lochner E, et al. Diabetes mellitus: long-term prognostic value of whole-body MR imaging for the occurrence of cardiac and cerebrovascular events. Radiology 2013;269(3):733, with permission.)

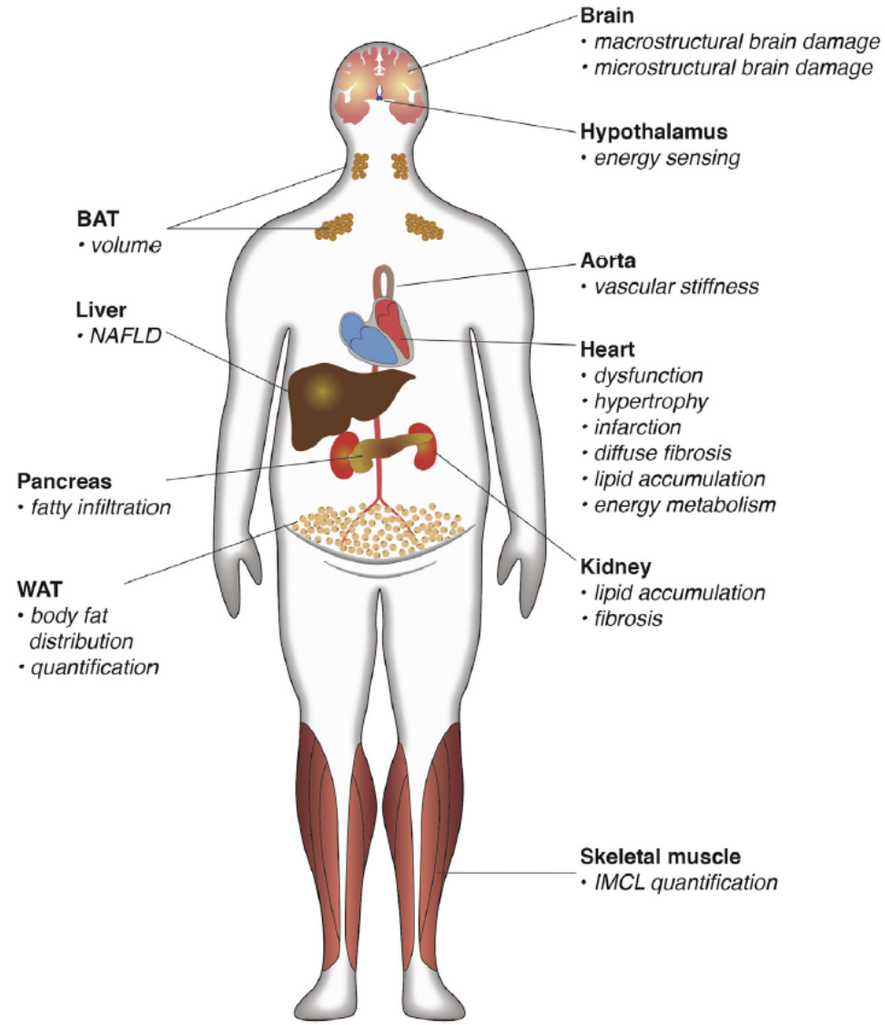

FIGURE 2. Overview of MR assessment of multi-organ involvement in metabolic syndrome. Key features of multiorgan involvement in the metabolic syndrome (MetS) that can be assessed with MR are shown. MRI accurately assesses the distribution of WAT showing an abundance of visceral adipose tissue (VAT) and peri-organ adipose tissue. In contrast, brown adipose tissue volume is diminished in obesity, suggesting that diminished thermogenesis may be involved in the etiology of MetS. Excessive accumulation of triglycerides in the liver, that is, hepatic steatosis, may play a central role in the development of MetS. Hepatic steatosis can progress into nonalcoholic steatohepatitis (NASH), fibrosis, and cirrhosis. Both excessive VAT and hepatic steatosis are strongly linked to insulin resistance, a key component of MetS. The cardiovascular system can be involved focally (eg, myocardial infarction) or globally (eg, diabetic cardiomyopathy). Cardiac remodeling of the cardiovascular system involves the sequelae of fatty infiltration, inflammation, fibrosis, and ultimately organ failure. Furthermore, brain involvement in MetS is increasingly being studied. In addition to macrostructural changes, such as brain atrophy and cerebral small vessel disease, microstructural changes are important features of MetS brain pathology. Various other organs, such as the kidney, pancreas, and skeletal muscle, undergo pathologic alterations in MetS patients. BAT, brown adipose tissue; WAT, white adipose tissue.

PURPOSE OF REVIEW

This review highlights MR techniques that assess multi-organ involvement in MetS.

ADIPOSE TISSUE

White Adipose Tissue

Abdominal visceral obesity Ectopic lipid accumulation in white adipose tissue (WAT) predominantly occurs in the visceral abdominal compartment. Visceral white adipocytes can contribute to MetS etiology by secreting excessive amounts of plasma free fatty acids, adipokines, and cytokines. MetS prevalence correlates with waist circumference, reflecting the role of abdominal obesity. However, waist circumference does not differentiate between subcutaneous adipose tissue (SAT) and visceral adipose tissue (VAT). Given that VAT has a stronger association with MetS than SAT, differentiation between SAT and VAT is critical.[3] Several MR techniques can be used to reliably quantify SAT and VAT. These include T1-weighted imaging, frequency-selective lipid imaging, and chemical-shift-encoded water–fat imaging, all different methods that can be lumped under the umbrella of water–fat MRI (Figures 3 and 4). An appropriate sequence can be chosen on the basis of local accessibility, available scanning time, and presence of image post-processing expertise. An overview of MR techniques for lipid quantification and their advantages/disadvantages is reviewed by Hu and Kan.[4]

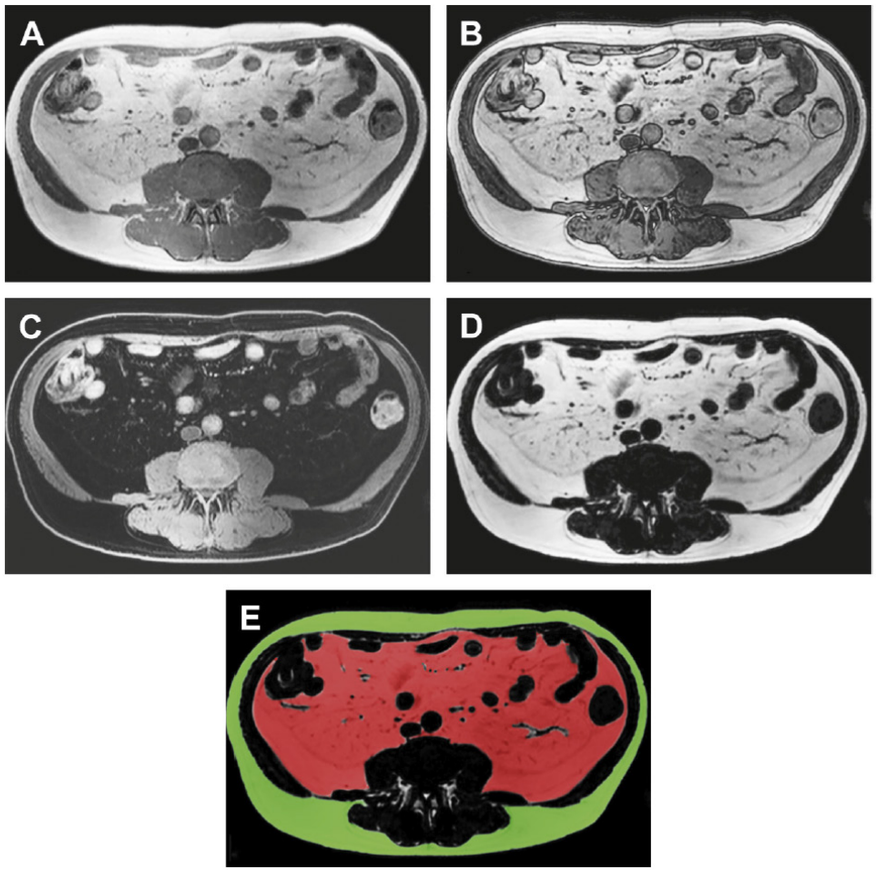

FIGURE 3. Chemical shift imaging of abdominal adipose tissue and subsequent volume quantification. Transverse slice at the level of L5 vertebra acquired with an mDIXON method using 2 echoes, **(A)** 1 in-phase and **(B)** 1 out-of-phase image. From these images, **(C)** a water image and **(D)** fat image can be reconstructed. **(E)** Image post processing can be used to semi automatically assess subcutaneous (green) and visceral (red) adipose tissue. This sequence was performed in a patient with longstanding type 2 diabetes mellitus showing relatively large amounts of visceral adipose tissue compared with subcutaneous adipose tissue.

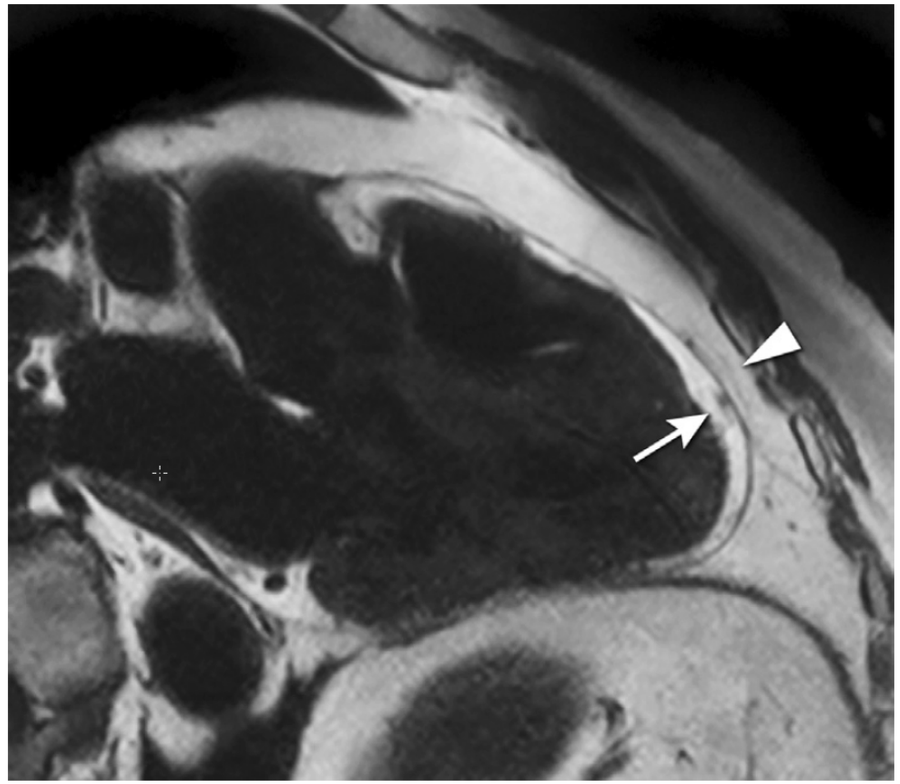

FIGURE 4. Frequency selective imaging of pericardial fat. Three-chamber view acquired with a turbo spin echo sequence with a spectral presaturation with inversion recovery (SPIR) and black blood prepulse sequence during 1 breath-hold at 3 T. This high-resolution sequence enables separate quantification of epicardial (arrow) and paracardial (arrowhead) fat volumes. Note the high paracardial fat mass in this male patient with type 2 diabetes mellitus. In addition to their different anatomic relation to coronary arteries, epicardial and paracardial fat have a different embryonic origin; epicardial fat has brown adipose tissue characteristics, whereas the paracardial fat does not. Therefore, separate quantification of epicardial and paracardial fat could reveal varying effects on end-organ damage.

Pericardial and perivascular fat

In addition to abdominal VAT, ectopic lipid accumulation around the heart (pericardial fat) and vessels (perivascular fat) is increased in MetS. Pericardial/perivascular fat is physiologically protective in terms of mechanical support and as a source of biochemical substrates, hormones, and cytokines. However, increased pericardial/perivascular lipid accumulation in MetS has been linked with low-grade systemic inflammation, adverse metabolic profile and risk of ischemic heart disease.[5] Various electrocardiogram-gated MR sequences, including steady-state free precession short axis sequences, fat-selective imaging (see Figure 4), and water–fat MRI, can be used to image pericardial fat and enable volume quantification in a reproducible manner.[1]

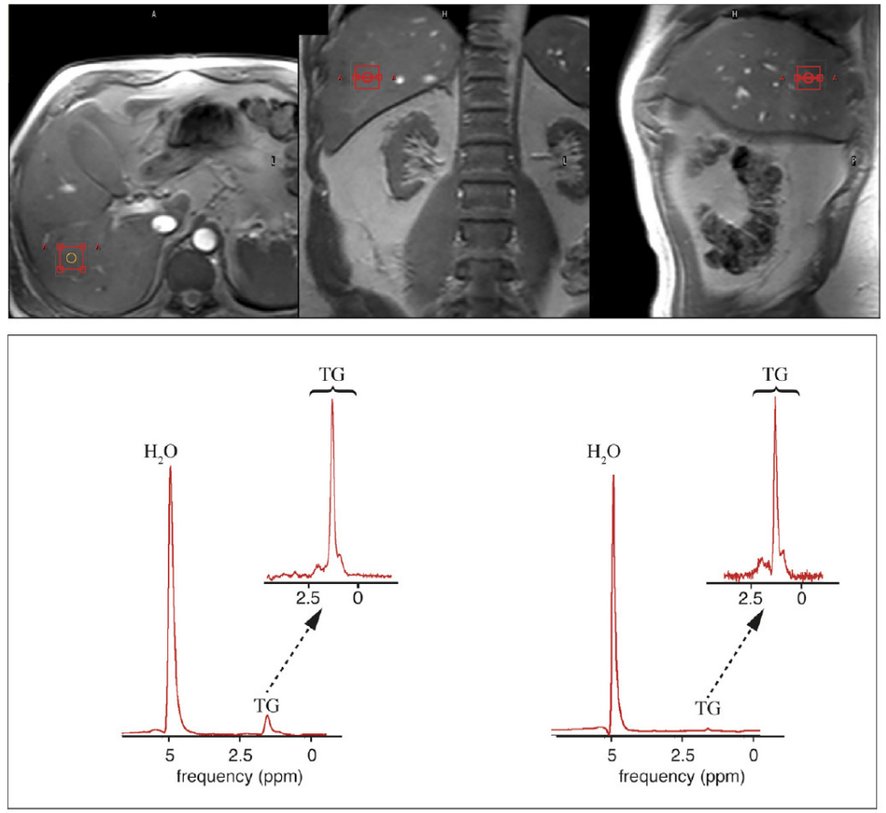

FIGURE 5. Proton magnetic resonance spectroscopy (^{1}H-MRS) of the liver to quantify hepatic triglyceride content. Voxel planning and examples of proton spectra acquired from the liver at 3 T. ^{1}H-MRS is based on the fact that different molecules have different chemical environments that translate to small differences in the strength of the magnetic field for the different metabolites. This effect is commonly known as chemical shift. In the recorded spectrum, the difference in magnetic field results in different resonance frequencies, expressed in parts per million (ppm) with respect to that of tetrametylsilane, for the various metabolites. In practice, 1 spectra without water suppression is recorded to use as an internal reference, and 1 or more with water suppression are acquired for quantification of triglycerides (TG). To be able to measure small metabolite levels, it is necessary to measure a volume much larger than the normal pixel size in MRI. Upper panel, Typical 8-mL voxel for liver ^{1}H-MRS. Lower panel, Acquired unsuppressed and water-suppressed spectra of an obese (left) and lean (right) volunteer. In liver spectra, TG is mainly represented by 3 different proton moieties, namely, CH_2-CH = CH-CH_2, $(-CH_2)^n$, and $-CH_3$. To quantify the fat percentage often the integrals below the $(-CH_2)^n$ and CH_3 peaks are summed and divided by the sum of the integrals of the water and $(-CH_2)^n$ and CH_3 peaks. In this example, the calculated hepatic triglyceride content was 8.26% for the obese subject and 1.24% for the lean subject.

Brown Adipose Tissue

In contrast to WAT, brown adipose tissue (BAT) volume and activity are diminished in obesity and may play a role in its development. BAT contributes significantly to total resting energy expenditure by dissipating glucose and free fatty acids into heat. The reference method for imaging BAT volume and activity is fluorodeoxyglucose PET-CT after mild cold exposure. The desire for a non-irradiating alternative has led to many MR techniques being evaluated to image BAT. These techniques identify BAT by its higher water fraction compared with WAT. However, MR of BAT is limited by the fact that, in humans, BAT and WAT are not entirely separated anatomically, complicating reliable BAT volume quantification. MRI of BAT activity is still in its infancy, although promising results using T2* imaging have been published recently.[4]

LIVER

Hepatic Steatosis

Ectopic lipid accumulation in the liver, that is, hepatic steatosis, is present in the majority of MetS patients and plays a central role in the pathogenesis of insulin resistance, hyperglycemia, and atherogenic dyslipidemia. The gold standard to determine hepatic steatosis is histology which requires a biopsy. However, several MR techniques can assess hepatic triglyceride (TG) content noninvasively with lower sampling error.[1] Currently, proton MRS (^{1}H-MRS) is the noninvasive gold standard to quantify hepatic TG content (Figure 5). ^{1}H-MRS has the best sensitivity for detection of small amounts of fat. A drawback of this technique is the risk of sampling error inherent to quantifying TG content in a small voxel.

Recently, the mDIXON technique using multiple echoes has been shown to enable liver fat quantification (Figure 6). By applying the mDIXON technique, T2* effects caused by the relatively high iron content in the liver can be compensated. The technique is becoming

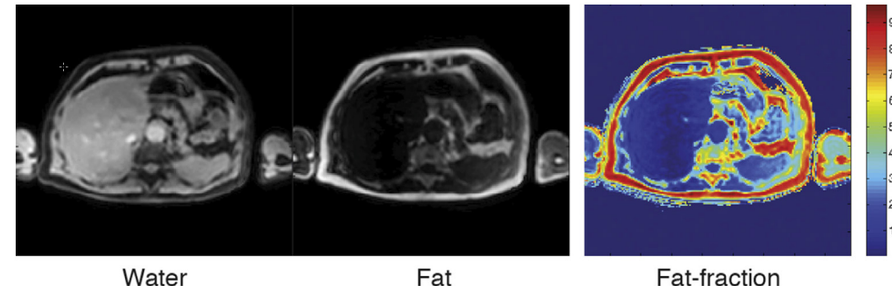

FIGURE 6. DIXON MRI of the liver to quantify hepatic triglyceride content. The left and middle images are the reconstructed water and fat images, respectively. A 6-point DIXON sequence was used with a starting echo time of 0.74 ms and echo spacing of 1 ms. The fat fraction was calculated on a pixel-by-pixel basis by dividing the fat image by the sum of the water and fat image. For this obese subject, the calculated fat fraction was between 3% and 9%, depending on the location, illustrating the inhomogeneous nature of hepatic steatosis.

increasingly popular because of its advantages of small sampling error (because it is a whole-organ imaging technique) and fast data acquisition.
Multidimensional chemical shift imaging is a multivoxel ^{1}H-MRS technique that measures a grid of multiple voxels, thus reducing sampling error. The disadvantage of chemical shift imaging is that data acquisition is slow and technically challenging.

Progression of Hepatic Steatosis into Inflammation, Fibrosis, and Cirrhosis
Hepatic steatosis can progress into nonalcoholic steatohepatitis, fibrosis, and ultimately cirrhosis and hepatic failure, a disease spectrum termed NAFLD. MRE, T1 mapping, phosphorus MRS (^{31}P-MRS), and diffusion-weighted imaging (DWI) are the focus of ongoing research to differentiate between NAFLD stages and explore potential advantages compared with histology, that is, lower sampling error and fewer complications.[6]
MRE (Figure 7) is an emerging technique that quantitatively images shear waves in the liver produced by external mechanical waves. A few validation studies have shown MRE's capability of differentiating between stages of NAFLD.[7]
T1 mapping is more readily available than MRE in terms of commercially available imaging sequences. This technique is based on the increased T1 relaxation time of edematous (nonalcoholic steatohepatitis) and fibrotic tissue. In NAFLD, several studies have been performed, showing a strong correlation between increasing T1 and increasing stages of fibrosis (see Figure 7).[8] In parallel with quantification of extracellular volume (ECV) expansion in cardiac imaging, ECV quantification in the liver is also feasible.[9] However, validation studies for ECV mapping to quantify liver fibrosis have yet to be published.
^{31}P-MRS can quantify metabolites involved in cell membrane metabolism as well as regulators of fibrosis pathogenesis can be assessed (Figure 8). Additionally, hepatic energy metabolism can be assessed by quantifying high energy phosphates.[10]
DWI is a promising technique that measures water movement in extracellular space. Unfortunately, DWI is less reliable in the presence of fat, which limits its use in NAFLD. Future studies must focus on correcting for the influence of fat in order for DWI to become suitable for NAFLD staging.[6]

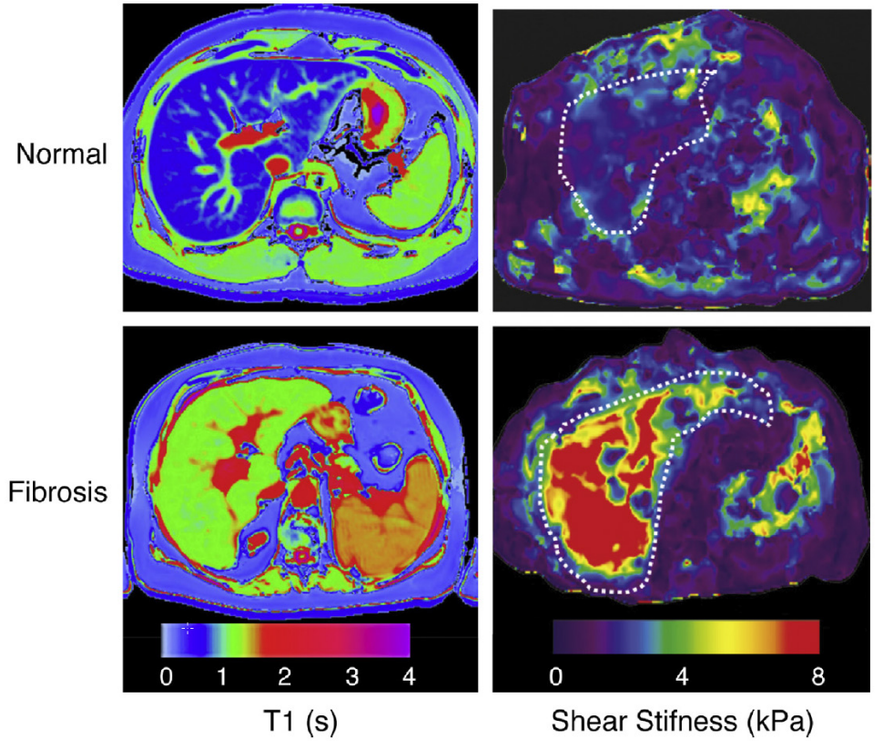

FIGURE 7. Magnetic resonance elastography and T1 mapping: Quantitative imaging of hepatic fibrosis in nonalcoholic fatty liver disease (NAFLD). Examples of T1 mapping (left) and magnetic resonance elastography (MRE; right) in healthy versus fibrotic liver tissue (as assessed by biopsy). T1 maps were acquired with a shortened modified Look-Locker (shMOLLI) sequence in a single breath-hold. Increasing T1 values were correlated with increasing degrees of fibrosis. MRE is performed using mechanical waves transmitted by an acoustic pressure driver. Using automated post-processing, data are translated into quantitative images displaying tissue shear stiffness in kPa. It has been shown that MRE is a useful tool to detect advanced stages of fibrosis. The dotted lines indicate the liver. (From [Left] Banerjee R, Pavlides M, Tunnicliffe EM, et al. Multiparametric magnetic resonance for the non-invasive diagnosis of liver disease. J Hepatol 2014;60(1):72, with permission; and [right] Kim D, Kim WR, Talwalkar JA, et al. Advanced fibrosis in nonalcoholic fatty liver disease: noninvasive assessment with MR elastography. Radiology 2013;268(2):415, with permission.)

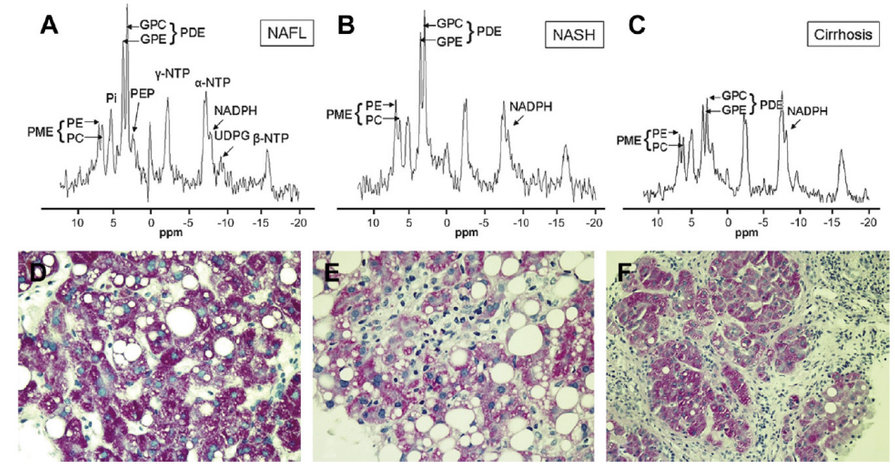

FIGURE 8. Phosphorus magnetic resonance spectroscopy (^{31}P-MRS) of the liver to differentiate between simple steatosis, steatohepatitis, and cirrhosis. Upper panel **(A–C)**, ^{31}P spectra, acquired at 3 T, of simple steatosis (nonalcoholic fatty liver [NAFL]), nonalcoholic steatohepatitis (NASH), and cirrhosis, respectively. This technique quantifies markers of hepatocyte membrane integrity. Corresponding liver biopsy specimens are shown in the lower panel **(D–F)**. The ratio of NADPH/(PME + PDE) was significantly lower in NAFL compared with NASH and cirrhosis, whereas the ratios of PE/(PME + PDE) and GPC/(PME + PDE) were higher in cirrhosis compared with NASH and NAFL. GPC, glycerophosphocholine; GPE, glycerophosphorylethanolamine; NADPH, nicotinamide adenine dinucleotide phosphate; NTP, nucleoside triphosphate; PC, phosphocholine; PDE, phosphodiester; PE, phosphosethanolamine; PEP, phosphoenolpyruvate; Pi, inorganic phosphate; PME, phosphomonoester; UDPG, uridine diphosphoglucose. (From Sevastianova K, Hakkarainen A, Kotronen A, et al. Nonalcoholic fatty liver disease: detection of elevated nicotinamide adenine dinucleotide phosphate with in vivo 3-T ^{31}P MR spectroscopy with proton decoupling. Radiology 2010;256(2):472; with permission.)

HEART

Cardiac MRI (anatomic, functional, angiography, perfusion, late gadolinium enhancement) is an important component in the assessment of a major complication of MetS, namely ischemic heart disease, which is reviewed elsewhere.[11] This section covers MR techniques to assess nonischemic remodeling in MetS, that is, "diabetic cardiomyopathy," which is characterized by diastolic dysfunction, hypertrophy, disrupted cardiac energy metabolism, and ECV expansion related to myocardial fibrosis.

Diastolic Dysfunction

Diastole comprises a combination of active (energy- consuming) relaxation and passive compliance. In MetS, diastolic dysfunction is an early feature and independent predictor of mortality. Diastolic dysfunction is caused by altered myocardial energetics and by diminished ventricular compliance.[1] MR using phase contrast imaging with velocity encoding is a robust technique to quantitatively assess diastolic function (Figure 9). Although the left ventricle (LV) has been the primary focus of research, recent findings show that right ventricular diastolic dysfunction is analogous to LV diastolic dysfunction.[12]

Hypertrophy

LV end-diastolic mass-to-volume ratio is tightly linked to markers of insulin resistance, indicating concentric LV remodeling in MetS.[11] Figure 9 shows an example of LV mass quantification with MR.

Cardiac Energy Metabolism

Cardiac energy metabolism is crucial for both systolic and diastolic function. As such, alterations in myocardial energetics may constitute the first step in heart failure pathophysiology.[13] MRS enables in vivo quantification of myocardial energetics (Figure 10).

Myocardial steatosis

An increased storage of TG in cardiomyocytes is a hallmark of diabetic cardiomyopathy.[1] As shown in animal studies, increased storage of myocardial TG reflects an abundance of toxic lipids that impair cardiomyocyte integrity and function. Myocardial steatosis may be an early sign of diabetic cardiomyopathy, because it is an independent predictor of diastolic dysfunction. Importantly, myocardial steatosis and diastolic dysfunction are reversible, signifying a window of opportunity for therapeutic interventions aimed at preventing overt heart failure.[1] MR is the only modality capable of quantifying myocardial TG content. Figure 11 shows an example of cardiac ^{1}H-MRS spectroscopy.

High-energy phosphate metabolism: fuel for function

The human heart requires enormous amounts of adenosine triphosphate (ATP) as a primary carrier of chemical energy. As such, the phosphocreatine/ ATP ratio is an important indicator of cardiac energy reserve and metabolic efficiency. A decreased ratio is associated with diastolic and systolic dysfunction. The finding that, in DM2 patients with normal cardiac mass and function, the phosphocreatine/ATP ratio was decreased compared with healthy controls, reflects the possibility that disruptions in myocardial energetics might play a role in the pathogenesis of cardiomyopathies.[13] Figure 12 shows an example of ^{31}P-MRS of the heart. Up to now, the use of cardiac ^{31}P-MRS has been limited to a research setting in experienced centers because of its complex acquisition.

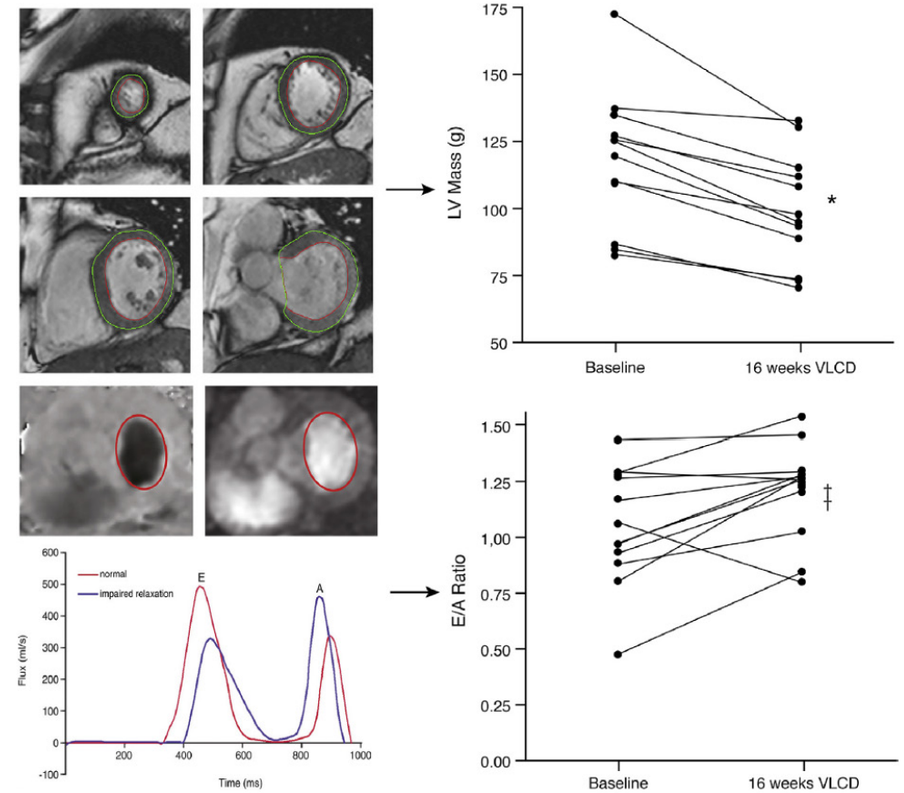

FIGURE 9. Reversible cardiac manifestations in metabolic syndrome: hypertrophy and diastolic dysfunction. MR measures left ventricular (LV) mass and diastolic function reliably and quantitatively, enabling detection of, for example, the effects of nutritional interventions in relatively small study populations. The upper left panel shows manual segmentation of myocardium in end-diastolic shorts axis images. Using dedicated software, LV mass can be calculated, showing that LV mass diminished in all type 2 diabetes mellitus patients after a 16-week very lowcalorie diet (VLCD). Decreased LV mass was tightly linked with improved diastolic function as reflected by an improved E/A ratio (E = early filling phase, A = atrial late filling phase). This parameter can be measured by using phase contrast MR with velocity encoding (lower right panel). By acquiring a 2-dimensional acquisition plane centered on the atrioventricular valve, a time–velocity or time–flow rate curve can be generated. Recent studies have shown an increased reliability of diastolic function assessment using 3-dimensional 3-directional velocity encoding with retrospective tracking to compensate for valve movement and changing flow direction throughout the cardiac cycle. * P < .001; † P < .05. (From [Left lower panel] van der Meer RW, Lamb HJ, Smit JW, et al. MR imaging evaluation of cardiovascular risk in metabolic syndrome. Radiology 2012;264(1):31, with permission; and [Right panel] Hammer S, Snel M, Lamb HJ, et al. Prolonged caloric restriction in obese patients with type 2 diabetes mellitus decreases myocardial triglyceride content and improves myocardial function. J Am Coll Cardiol 2008;52(12):1011, with permission.)

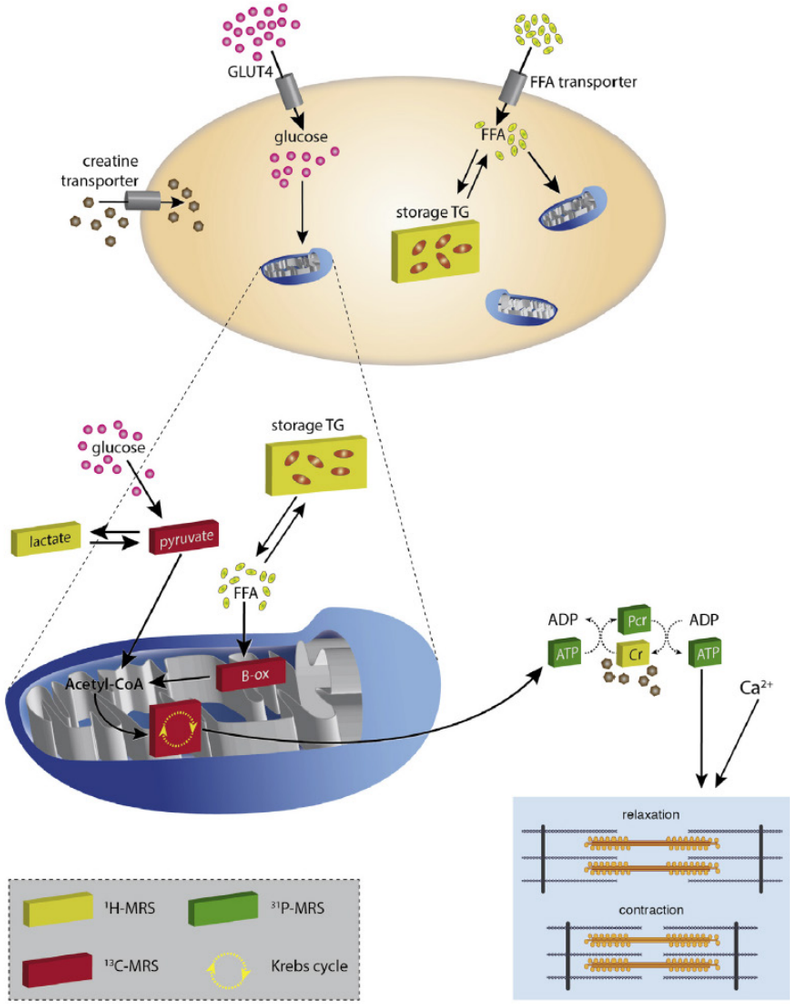

FIGURE 10. MR spectroscopy assessment of cardiac energy metabolism. The cardiomyocyte is represented in orange. FFAs and glucose, in a ratio of 3:1, are the primary sources of chemical energy for the production of ATP, which takes plays in the mitochondrion (blue). FFAs are either stored as TGs or oxidized (B-ox) to give acetyl-CoA. Glucose is glycolysed—in the presence of oxygen—to pyruvate, another substrate for acetyl-CoA, which enters the Krebs cycle for oxidative phosphorylation. This process provides energy required to form ATP. In the mitochondrion, ATP and Cr give rise to phosphocreatine (PCr), which diffuses to the myofibril, where it is converted into mechanical energy, under tight control of the Ca^{2+} flux. Note here that both systole and diastole require ATP. The colored boxes (yellow, green, and red) indicate opportunities for measurement with ^{1}H, ^{31}P and ^{13}C MRS, respectively. For ^{1}H and ^{31}P, see also Figures 15 and 16. Cardiac ^{13}C-MRS has not yet been performed in humans, but animal studies using hyperpolarized metabolic tracers have shown the feasibility of using cardiac ^{13}C-MRS to assess fuel flux (B-ox, Krebs cycle, pyruvate). Acetyl-CoA, acetyl-coenzyme A; ADP, adenosine diphosphate; ATP, adenosine triphosphate; B-ox, ß-oxidation; Ca^{2+}, ionized calcium; Cr, creatine; FFA, free fatty acid; GLUT4, glucose transporter type 4; PCr, phosphocreatine; TG, triglyceride content. (From Bizino MB, Hammer S, Lamb HJ. Metabolic imaging of the human heart: clinical application of magnetic resonance spectroscopy. Heart 2014;100(11):881–90; with permission.)

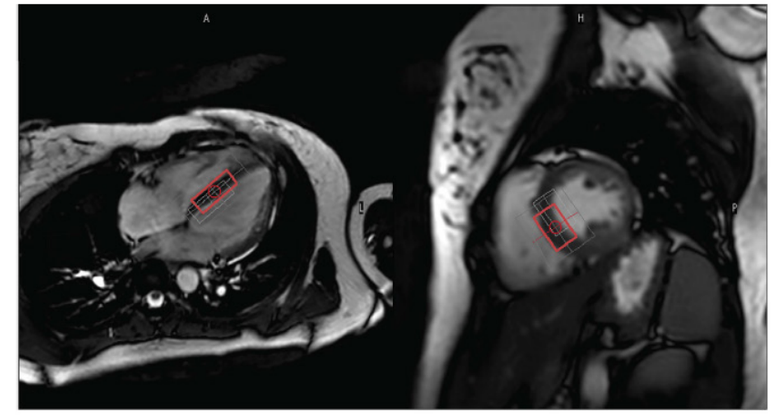

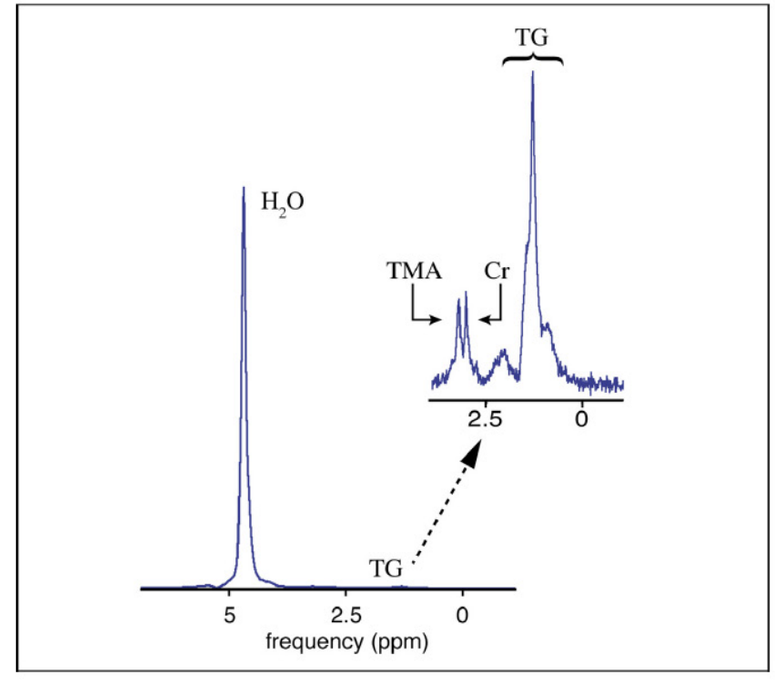

FIGURE 11. Cardiac proton magnetic resonance spectroscopy (^{1}H-MRS) to quantify myocardial steatosis. Cardiac ^{1}H-MRS was performed on 1.5 and 3 T MR systems using commercially available transceiver coils, and recently at 7 T using custom-built detectors. Cardiac ^{1}H-MRS is subject to motion artifacts owing to contraction and breathing. To overcome these issues, cardiac ^{1}H-MRS is usually performed with electrocardiographic gating and either breath-holding or free breathing with respiratory motion triggering/compensation. To prevent contamination of pericardial fat, the voxel of interest (VOI) is placed in the interventricular septum. The most commonly used pulse sequences are stimulated echo acquisition mode (STEAM) and point resolved spectroscopy (PRESS). The low abundance of the various metabolites requires water suppression and acquisition of multiple averages resulting in relatively long scan duration. The water-suppressed spectrum displayed in the lower panel shows signals from creatine (Cr), triglycerides (TG) and trimethyl ammonium (TMA). In this example, 16 non–water-suppressed and 48 water-suppressed averages were acquired at 3 T from a VOI of 15 mL.

Extracellular Volume Expansion

Another hallmark of diabetic cardiomyopathy is ECV expansion caused by collagen deposition, referred to as myocardial fibrosis. Fibrosis is associated with mortality and activation of the renin– angiotensin–aldosterone system[11] and can be quantified using a modified Look Locker (MOLLI) or shortened MOLLI sequence.[14,15] Using these sequences, native T1 mapping and postcontrast T1 mapping can be performed. By combining these images, fractional ECV can be quantified (Figure 13).

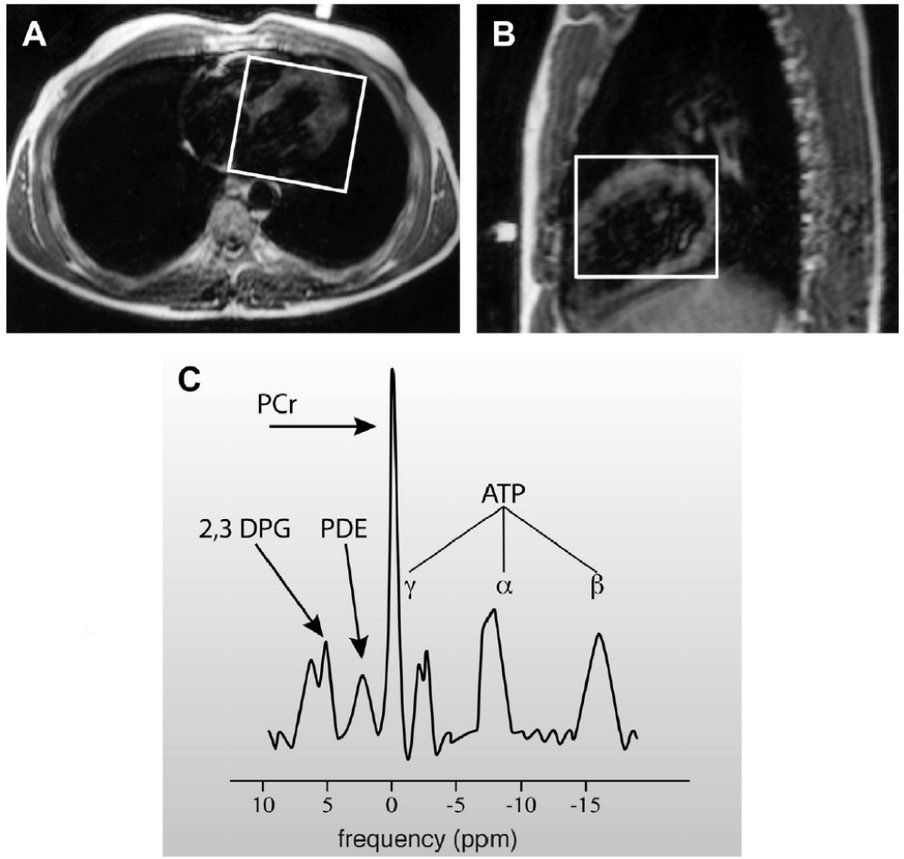

FIGURE 12. Cardiac phosphorus magnetic resonance spectroscopy [^{31}P-MRS] to assess high-energy phosphates. Cardiac ^{31}P-MRS at 1.5 T is performed by positioning a volume of interest (square box) over almost the entire heart **(A, B)**; eliminating signal contamination from skeletal muscle is essential. The PCr/ATP ratio can be calculated from the spectrum **(C)** and is an important representation of cardiac energy reserve. In the metabolic syndrome (MetS), a decreased PCr/ATP ratio has been found before the onset of overt heart failure. ATP, adenosine triphosphate; 2,3 DPG, 2,3-diphosphglycerate; PCr, phosphocreatine; PDE, phosphodiesters; ppm, parts per million. (From Bizino MB, Hammer S, Lamb HJ. Metabolic imaging of the human heart: clinical application of magnetic resonance spectroscopy. Heart 2014;100(11):881–90; with permission.)

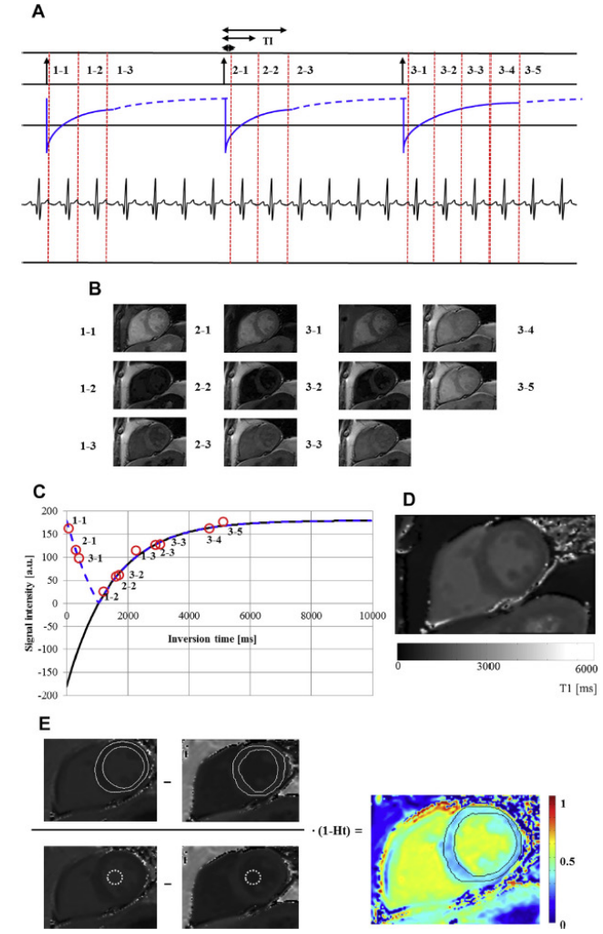

FIGURE 13. MR acquisition and image after processing to evaluate fibrosis in diabetic cardiomyopathy. Modified Look Locker inversion recovery (MOLLI) sequence to determine T1 values of myocardium and subsequent use of precontrast and postcontrast T1 maps to calculate extracellular volume, acquired at 3 T. **(A)** The MOLLI experiment. This technique consists of 3 consecutive electrocardiogram triggered look locker (LL) experiments, with a three (1), three (2), and five (3) segment single-shot readout. Between each LL experiment, 4 heartbeats are used for magnetization recovery. **(B, C)** In total, within a 17–heartbeat breath-hold, the longitudinal relaxation curve is sampled at 11 different inversion times. The images are reordered based on increasing inversion time, that is, the time between the inversion pulse and the readout. **(D)** The T1 map can be calculated by performing voxel wise fitting the signal intensity (SI): $SI[a.u.]=A-B\times e^{-TI/T_1^*}$, $T_1=T_1^*((B/A)-1)$. A commonly used variation on the MOLLI method is the shortened MOLLI (ShMOLLI), where only 2 consecutive electrocardiograph-triggered LL experiments are performed with a 5 and 1 single shot read out. (E) The formula used to calculate the extracellular volume fraction (ECV):

$$ECV_{myo}=\frac{R_{1,post,myo}-R_{1,pre,myo}}{R_{1,post,blood}-R_{1,pre,blood}}(1-H_t).$$

The ECV is determined with a combination of native and postcontrast T1 mapping. The gadolinium-based contrast agent will distribute in the extracellular space of the myocardium. Therefore, a higher concentration of gadolinium indicates a larger ECV, which could indicate more fibrosis. In the example given in this figure, acquired in a 66-year-old type 2 diabetes mellitus patient with myocardial infarction, the average ECV of the myocardium was 0.34, or 34%, compared with 27% in healthy volunteers.

BRAIN INVOLVEMENT IN THE METABOLIC SYNDROME

Brain Structures Involved in Feeding Behavior

Multiple brain structures are functionally involved in the regulation of food intake. Homeostatic regulation of food intake is driven by inputs from the basal ganglia, thalamus, and hippocampus. Interestingly, a recent study found increased amygdalar and hippocampal volumes, as assessed by 3-dimensional T1-weighted MRI, in elderly obese individuals.[16] The finding that these morphometric changes occurred in the amygdala and hippocampus but not in other brain structures that play a role in feeding behavior suggests that cognitive aspects may be of major importance in the regulation of feeding.[16] Additional studies are required to examine the mechanisms behind the observed morphometric changes.

Blood oxygen level–dependent (BOLD) functional MRI is a sensitive marker of brain activation. It has been shown previously that healthy, lean volunteers demonstrated a significant dose dependent decrease of the BOLD signal in the hypothalamus after glucose ingestion.[17] In patients with DM2, hypothalamic neuronal activity is altered, as demonstrated by the absence of a BOLD signal decrease after glucose ingestion.[18] Recently it has been shown that after following a very low-calorie diet for 4 days, the hypothalamus in DM2 patients responds to glucose ingestion similarly to that in healthy subjects.[19] Because the hypothalamus is involved in the control of postprandial metabolism, this may explain the strong metabolic improvement that can be observed in DM2 patients upon caloric restriction.[19] Future studies are needed to elucidate the fundamental mechanisms behind the hypothalamic response to glucose ingestion.

Structural Brain Damage

Although cardiovascular disease is considered to be the main long-term complication of MetS, multiple organs may be affected, including the brain.[1] Risk factors associated with MetS accelerate cerebral small vessel disease, which may result in white matter lesions, cerebral microbleeds, and brain atrophy, as detected by conventional structural MRI.[20] Subtle microstructural brain damage may occur in the normal appearing brain tissue in the absence of overt brain abnormalities.[21]

DTI is an MRI technique that is well suited to detect early microstructural changes in normal appearing brain tissue in a number of disease states. Using DTI, Shimoji and colleagues[22] recently found that fractional anisotropy (FA) values were lower in MetS subjects relative to control subjects. FA reflects the "coherence" of highly structured tissue, such as axon bundles. Accordingly, lower FA values indicate microstructural brain tissue decline. Regional brain analysis showed that mean FA values of the right inferior fronto-occipital fasciculus were lower in MetS subjects compared with controls subjects.[22] The inferior fronto-occipital fasciculus connects all 4 major lobes of the brain and may play an important role in linking all the components of what is commonly referred to as the social brain. The social brain hypothesis may in turn be related to human feeding behavior; several functional MRI studies have detected a correlation between neural activity and eating behavior.

Magnetization transfer imaging is another sensitive MRI technique that can be used to evaluate changes in brain microstructure.[23] Using both DTI and magnetization transfer imaging, Sala and colleagues[21] recently showed that clustering of risk factors in MetS is associated with evidence of microstructural damage in the gray and white matter as indicated by a decreased magnetization transfer ratio histogram peak height and increased mean diffusivity. Voxel-wise analysis of cortical gray matter magnetization transfer ratio showed that changes were diffuse and symmetric in both hemispheres. Future longitudinal studies should determine whether these changes evolve into more pronounced structural deterioration or changes in cognition.

Arterial Stiffness

Pulse wave velocity (PWV) is a surrogate marker of vascular stiffness. It is defined as the velocity of the systolic wave front propagating through the vessels (Figure 14) with increased PWV, indicating arterial wall stiffening. MRI enables PWV assessment in different vascular territories, including the aortic arch and the carotid arteries. By using MRI, Roes and colleagues[24] found that aortic PWV was increased in MetS subjects. Another study found that aortic PWV is associated with LV mass and lacunar brain infarcts in hypertensive patients.[25] These observations may be explained by the concept that aortic stiffening increases exposure of the microcirculation to abnormal physical forces that may lead to endorgan damage.[26] MRI enables a comprehensive evaluation of the heart, large vessels, and brain. Future studies should focus on the pathogenesis of end-organ damage in MetS, and evaluate the effect of interventions.

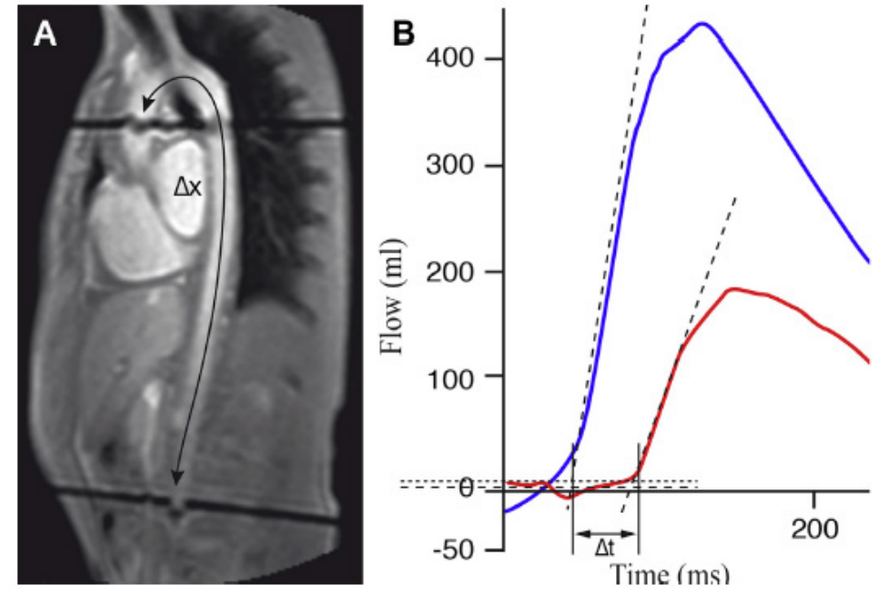

FIGURE 14. MR assessment of arterial stiffness: Pulse wave velocity (PWV). Through-plane velocity encoded MRI assessment of PWV at 1.5 T. **(A)** Sagittal gradient-echo image aligned with the long axis of the aorta shows 2 perpendicular image acquisition planes through the ascending aorta and abdominal aorta. The path length is indicated by Δx. **(B)** Velocity curves are used to assess the time delay (Δt) of the arrival of the proximal (blue curve) and abdominal flow (red curve). The PWV is calculated as Δx/Δt.

OTHER ORGANS

Kidney

The relationship between MetS and chronic kidney disease (CKD) has become increasingly clear over the past years. Even before the onset of overt diabetes or hypertension, patients have an increased risk of microalbuminuria and renal insufficiency. CKD pathophysiology involves accumulation of toxic lipids, inflammation, neurohumoral factors, and ultimately fibrosis.[27] MR assessment of renal TG content (RTGC) was performed in diabetic mice, using chemical shift-selective imaging in combination with BOLD MRI. The results showed that RTGC was inversely correlated with intrarenal oxygenation, suggesting a possible causal link between RTGC and CKD.[28] Recently, it has been shown that human RTGC can be assessed reliably with ^{1}H-MRS (Figure 15).[29] Therefore, renal ^{1}H-MRS provides a tool to study the association between RTGC, MetS, and CKD in humans. As a final common pathway of CKD in MetS, quantitative imaging of renal fibrosis—in parallel with heart and liver—with MR is an obvious next step. To this end, several methods, such as quantitative susceptibility mapping and renal T1 mapping, are promising.[30]

Pancreas

In parallel with NAFLD, fatty pancreas is associated with visceral obesity and hypertriglyceridemia. This was shown in a population study using iterative decomposition of water and fat with echo asymmetry and least squares estimation (IDEAL), which is a DIXON-based technique with 3 echoes to account for both B_0 and B_1 magnetic field inhomogeneities.[31] Further studies are needed to clarify the role of fatty pancreas in MetS pathophysiology.

Skeletal Muscle

An increased level of intramyocellular lipids, without a corresponding increase in extramyocellular lipids, is a key feature of peripheral insulin resistance, that may play a role in the increased hepatic steatosis and dyslipidemia, observed in MetS.[32,33] ^{1}H-MRS is the only technique sensitive enough to differentiate intramyocellular lipids from extramyocellular lipids (Figure 16). Using ^{31}P-MRS, skeletal muscle phosphate–ATP flux can be assessed, thereby providing insight into mitochondrial (dys)function and its relationship with insulin sensitivity.[34]

SUMMARY

MR is a powerful, noninvasive tool to assess multiorgan involvement in MetS. Key elements of MetS pathophysiology, ranging from ectopic lipid accumulation to end-organ damage of liver, heart, brain, kidney, pancreas, and skeletal muscle, can be evaluated using a multitude of MR techniques. As such, MR has proven its utility with respect to unraveling MetS pathophysiology, as well as monitoring efficacy of therapeutic interventions.

ACKNOWLEDGMENT

The authors thank G. Kracht for figure composition and layout.

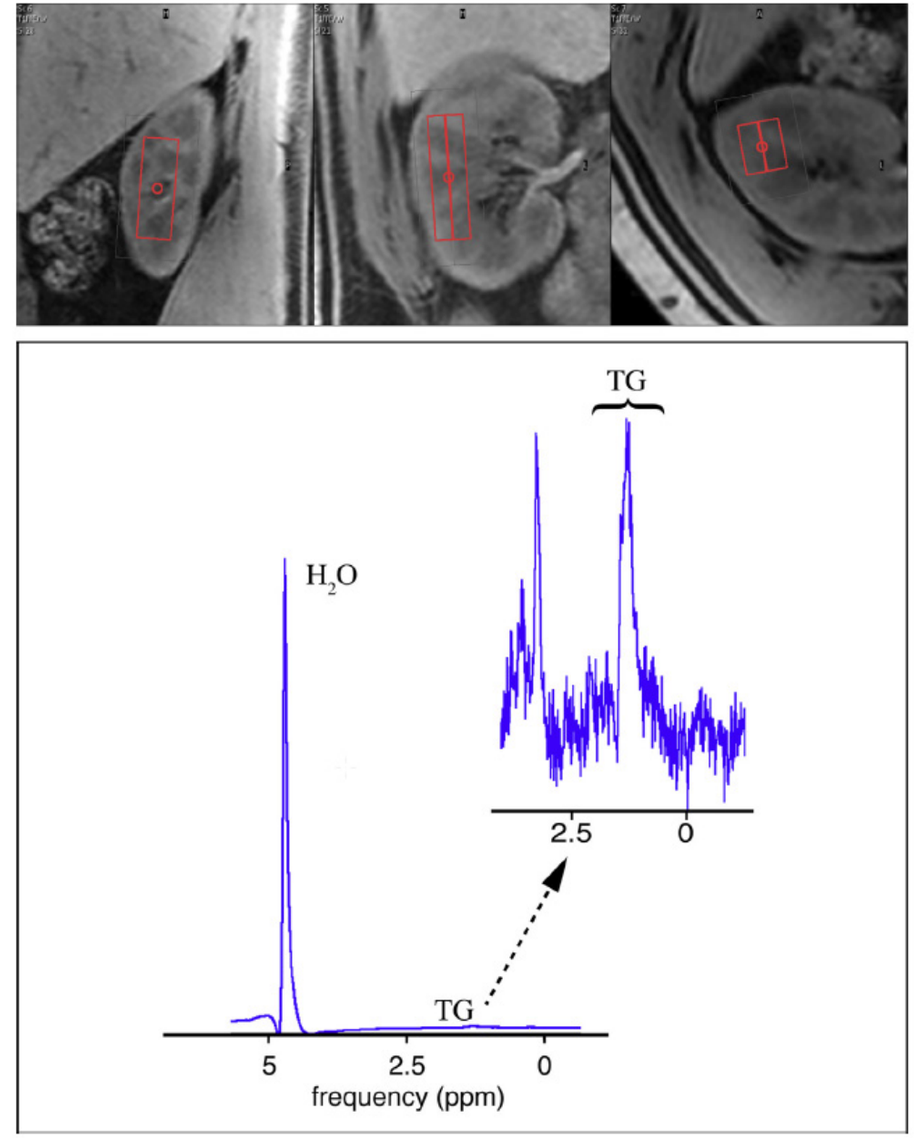

FIGURE 15. Proton magnetic resonance spectroscopy (^{1}H-MRS) for the evaluation of renal steatosis. MR spectra of the kidney at 3 T. Sixteen water spectra and 64 water-suppressed breath-hold spectra were acquired with a PRESS sequence from a 4-mL voxel. The renal fat fraction in this healthy volunteer was 0.28%. Compared with liver, lipid levels are lower, and also owing to the smaller organ size, the voxel of interest (VOI) must be smaller; both result in lower signal-to-noise ratio (SNR) in the kidney, requiring greater signal averaging. TG, triglycerides; ppm, parts per million.

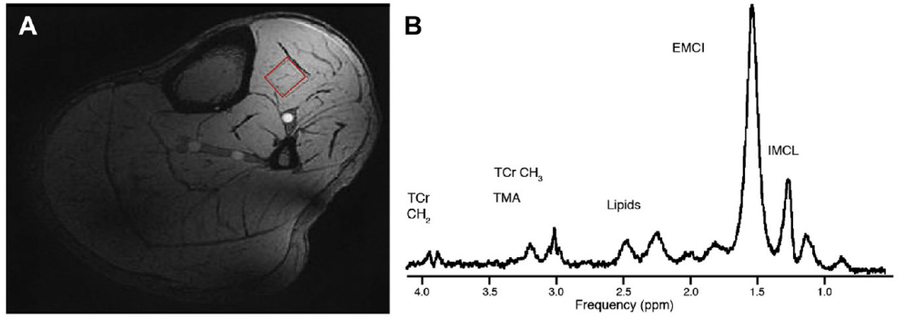

FIGURE 16. Skeletal muscle proton magnetic resonance spectroscopy (^{1}H-MRS) at 7 T. **(A)** The red box shows the voxel of interest in the tibialis anterior muscle of a healthy volunteer scanned on a 7 T system. **(B)** The corresponding ^{1}H spectrum shows clear separation of intramyocellular lipids (IMCL) and extramyocellular lipids (EMCL). IMCL is strongly linked to insulin resistance, whereas EMCL is not. Other peak assignments: tCr, total creatine (CH_2 and CH_3 resonances); TMA, tri-methyl ammonium.

REFERENCES

1. van der Meer RW, Lamb HJ, Smit JW, et al. MR imaging evaluation of cardiovascular risk in metabolic syndrome. Radiology 2012;264(1):21–37.

2. Bamberg F, Parhofer KG, Lochner E, et al. Diabetes mellitus: long-term prognostic value of whole-body MR imaging for the occurrence of cardiac and cerebrovascular events. Radiology 2013;269(3):730–7.

3. Despres JP, Lemieux I. Abdominal obesity and metabolic syndrome. Nature 2006;444(7121):881–7.

4. Hu HH, Kan HE. Quantitative proton MR techniques for measuring fat. NMR Biomed 2013; 26(12):1609–29.

5. Iozzo P. Myocardial, perivascular, and epicardial fat. Diabetes Care 2011;34(Suppl 2):S371–9.

6. Cobbold JF, Patel D, Taylor-Robinson SD. Assessment of inflammation and fibrosis in non-alcoholic fatty liver disease by imaging-based techniques. J Gastroenterol Hepatol 2012;27(8):1281–92.

7. Kim D, Kim WR, Talwalkar JA, et al. Advanced fibrosis in nonalcoholic fatty liver disease: noninvasive assessment with MR elastography. Radiology 2013;268(2):411–9.

8. Banerjee R, Pavlides M, Tunnicliffe EM, et al. Multiparametric magnetic resonance for the noninvasive diagnosis of liver disease. J Hepatol 2014; 60(1):69–77.

9. Bandula S, Banypersad SM, Sado D, et al. Measurement of Tissue interstitial volume in healthy patients and those with amyloidosis with equilibrium contrast-enhanced MR imaging. Radiology 2013; 268(3):858–64.

10. Sevastianova K, Hakkarainen A, Kotronen A, et al. Nonalcoholic fatty liver disease: detection of elevated nicotinamide adenine dinucleotide phosphate with in vivo 3-T 31P MR spectroscopy with proton decoupling. Radiology 2010;256(2):466–73.

11. Shah RV, Abbasi SA, Kwong RY. Role of cardiac MRI in diabetes. Curr Cardiol Rep 2014;16(2):449.

12. Widya RL, van der Meer RW, Smit JW, et al. Right ventricular involvement in diabetic cardiomyopathy. Diabetes Care 2013;36(2):457–62.

13. Bizino MB, Hammer S, Lamb HJ. Metabolic imaging of the human heart: clinical application of magnetic resonance spectroscopy. Heart 2014; 100(11):881–90.

14. Messroghli DR, Radjenovic A, Kozerke S, et al. Modified look-locker inversion recovery (MOLLI) for high-resolution T1 mapping of the heart. Magn Reson Med 2004;52(1):141–6.

15. Piechnik SK, Ferreira VM, Dall'Armellina E, et al. Shortened modified look-locker inversion recovery (ShMOLLI) for clinical myocardial T1-mapping at 1.5 and 3 T within a 9 heartbeat breathhold. J Cardiovasc Magn Reson 2010;12:69.

16. Widya RL, de Roos A, Trompet S, et al. Increased amygdalar and hippocampal volumes in elderly obese individuals with or at risk of cardiovascular disease. Am J Clin Nutr 2011;93(6):1190–5.

17. Smeets PA, de GC, Stafleu A, et al. Functional MRI of human hypothalamic responses following glucose ingestion. Neuroimage 2005;24(2):363–8.

18. Vidarsdottir S, Smeets PA, Eichelsheim DL, et al. Glucose ingestion fails to inhibit hypothalamic neuronal activity in patients with type 2 diabetes. Diabetes 2007;56(10):2547–50.

19. TeeuwisseWM,WidyaRL, PaulidesM, et al.Short-term caloric restriction normalizes hypothalamic neuronal responsiveness to glucose ingestion in patients with type 2 diabetes. Diabetes 2012;61(12):3255–9.

20. Kloppenborg RP, Nederkoorn PJ, Grool AM, et al. Cerebral small-vessel disease and progression of brain atrophy: the SMART-MR study. Neurology 2012;79(20):2029–36.

21. Sala M, de RA, Berg AV, et al. Microstructural brain tissue damage in metabolic syndrome. Diabetes Care 2014;37(2):493–500.

22. Shimoji K, Abe O, Uka T, et al. White matter alteration in metabolic syndrome: diffusion tensor analysis. Diabetes Care 2013;36(3):696–700.

23. Seiler S, Cavalieri M, Schmidt R. Vascular cognitive impairment - an ill-defined concept with the need to define its vascular component. J Neurol Sci 2012;322(1–2):11–6.

24. Roes SD, Alizadeh DR, Westenberg JJ, et al. Assessment of aortic pulse wave velocity and cardiac diastolic function in subjects with and without the metabolic syndrome: HDL cholesterol is independently associated with cardiovascular function. Diabetes Care 2008;31(7):1442–4.

25. Brandts A, van Elderen SG, Westenberg JJ, et al. Association of aortic arch pulse wave velocity with left ventricular mass and lacunar brain infarcts in hypertensive patients: assessment with MR imaging. Radiology 2009;253(3):681–8.

26. Mitchell GF, van Buchem MA, Sigurdsson S, et al. Arterial stiffness, pressure and flow pulsatility and brain structure and function: the age, gene/environment susceptibility – Reykjavik study. Brain 2011; 134(Pt 11):3398–407.

27. Singh AK, Kari JA. Metabolic syndrome and chronic kidney disease. Curr Opin Nephrol Hypertens 2013; 22(2):198–203.

28. Peng XG, Bai YY, Fang F, et al. Renal lipids and oxygenation in diabetic mice: noninvasive quantification with MR imaging. Radiology 2013;269(3): 748–57.

29. Hammer S, de Vries AP, de Heer P, et al. Metabolic imaging of human kidney triglyceride content: reproducibility of proton magnetic resonance spectroscopy. PLoS One 2013;8(4):e62209.

30. Xie L, Sparks MA, Li W, et al. Quantitative susceptibility mapping of kidney inflammation and fibrosis in type 1 angiotensin receptor-deficient mice. NMR Biomed 2013;26(12):1853–63.

31. Wong VW, Wong GL, Yeung DK, et al. Fatty pancreas, insulin resistance, and beta-cell function: a population study using fat-water magnetic resonance imaging. Am J Gastroenterol 2014;109(4): 589–97.

32. Flannery C, Dufour S, Rabol R, et al. Skeletal muscle insulin resistance promotes increased hepatic de novo lipogenesis, hyperlipidemia, and hepatic steatosis in the elderly. Diabetes 2012;61(11):2711–7.

33. Boesch C, Machann J, Vermathen P, et al. Role of proton MR for the study of muscle lipid metabolism. NMR Biomed 2006;19:968–88.

34. Kemp GJ, Brindle KM. What do magnetic resonance-based measurements of Pi – ATP flux tell us about skeletal muscle metabolism. Heart Fail Rev. 2013;18:657–668.